Astron. Astrophys. 333, 1016–1024 (1998)

ASTRONOMY
AND
ASTROPHYSICS

PP 13S, a young, low-mass FU Orionis-type pre-main sequence star

Göran Sandell[1] **and Colin Aspin**[2]

[1] Joint Astronomy Centre, 660 N. A'ohōkū Place, Hilo, HI 96720, USA
[2] Nordic Optical Telescope, Apartado 474, E-38700 Santa Cruz de la Palma, Canarias, Spain

Received 29 December 1997 / Accepted 4 February 1998

Abstract. We present near-IR imaging and spectroscopy, together with sub-mm/mm photometry and ^{12}CO molecular line maps of the cometary nebula PP 13S. Previous models have been unable to resolve whether PP 13S is a young, pre-main sequence star or an old, evolved object. Our new observations prove conclusively that PP 13S is a young stellar object with a luminosity of $\sim$30 $L_\odot$ and an accretion disk with an inclination of $\sim 40°$. It has a ^{12}CO J=2–1 outflow, strong and broadened CO overtone band absorption, and vibrationally excited H_2 emission. We conclude that PP 13S has all the characteristics of an FU Orionis-type star, and although no outburst has been observed, we suggest that PP 13S should be added to the list of FUor pre-main sequence stars. Our study also includes PP13N, which we resolve into a young double star system.

Key words: ISM: individual objects: PP 13S – ISM: jets and outflows – stars: pre-main sequence – infrared: ISM: lines and bands – radio continuum: ISM – radio lines: ISM

1. Introduction

PP13 (Parsamian & Petrossian 1979) appears on optical images as a red fan-shaped bipolar nebula embedded in the dark cloud L1473. It was first studied in detail by Cohen et al. (1983) who concluded that the cometary nebula was associated with a bright IR source designated PP 13S, and that an apparently associated northern component, PP13N, although on the symmetry axis of the nebula, was an unrelated cool T Tauri-like star. PP 13S is completely obscured in the visible and has unusually large ice and silicate absorption at 3 and 10 μm. Cohen at al. attribute this to absorption in a cool edge-on dust disk around PP 13S. Although Cohen et al. favor the interpretation of PP 13S as a very young T Tauri star, they did not exclude the possibility that it could be an evolved low-mass star. Smith (1993) present additional near-IR spectroscopy and imaging. His analysis also favored a PMS nature for PP 13S. Tapia et al. (1997), who did optical CCD and near-IR imaging of a sample of small optical nebulae associated with IRAS sources, concluded that PP 13S is a young Class I type object.

Send offprint requests to: Göran Sandell

We originally included PP13 in a survey of (sub)mm continuum emission from T Tauri stars. In that survey, PP 13S was easily detected at 800 μm and was subsequently mapped at both 800 and 450 μm. To shed further light on its nature, we have also obtained new ^{12}CO molecular line maps and high resolution J, H, K and narrow-band (nb)L images of the region. It is these data, together with 2 μm spectra and thermal IR photometry, that we present below.

2. Observations and data reduction

2.1. Near- and mid-IR imaging and photometry

Near-IR (NIR) J, H, K and narrow band L (nbL, 6%, 3.4 μm) images of the PP13 region centred on the coordinates $\alpha = 04^h\ 07^m\ 21.2^s$, $\delta = +38°\ 00'\ 08''$ (1950.0), were taken on the United Kingdom Infrared Telescope[1], Mauna Kea, Hawaii (UT 27 December 1993) using the 2D array camera IRCAM. At the time, the camera was based on a 58×62 Santa Barbara Research Center (SBRC) InSb array allowing a wavelength coverage from 1–5 μm. IRCAM is described in detail in McLean et al. (1986). A scale of 0.62″/pixel was used for the observations. Conditions throughout the observing run were photometric with seeing $\sim$1″. The data on PP13 was calibrated by observing the UKIRT standard star HD40335 (J=6.55, H=6.47, K=6.45, L=6.43). More details of the data reduction techniques can be found in Aspin et al. (1993). The J and K band images obtained are shown in Fig. 1.

M band photometry of PP 13S was obtained at UKIRT (UT 28 December 1993) using the NIR single channel aperture photometer, UKT9, with a 5″ aperture. Photometric calibration was performed using the UKIRT standards BS1713 (M=0.09) and BS2943 (M=-0.06). N (10 μm) and Q (19.5 μm) photometry of PP 13S were earlier obtained at UKIRT (UT 18 November 1993) using the mid-IR single channel aperture photometer, UKT8, with a 6″ aperture. Photometric calibration of this data was performed via observations of the UKIRT standards and BS1708 (N=-1.94, Q=-1.93) and BS2491 (N=-1.42, Q=-1.36). The results of the photometry on the PP13 sources are shown in Table 1.

[1] operated by the Joint Astronomy Centre on behalf of the United Kingdom Particle Physics and Astronomy Research Council (PPARC)

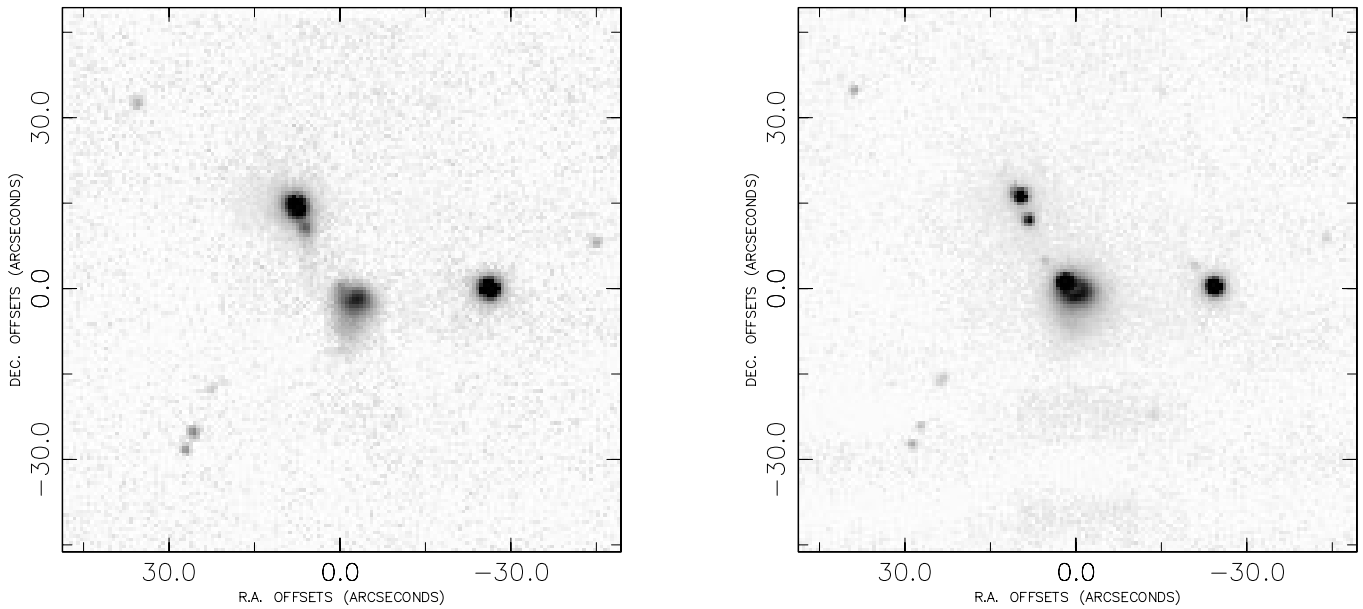

Fig. 1. J (left) and K (right) band images of the PP13 region. PP 13S is at the origin (0,0) while the double star system PP13 Na,b is offset $\sim$ 10″ to the north–east. In J, the embedded stellar object is just detected at the apex of the diffuse reflection nebulosity. In K, a bright source is seen at this position. The star $\sim$30″ west of PP 13S is PP 13W. The faint point-like sources seen $\sim$ 3″ to the north-east of both PP 13S$*$ and PP13W in the K image are ghosts.

2.2. Near-IR spectroscopy

The NIR spectroscopy presented below was obtained using the cooled grating array spectrometer, CGS4, on UKIRT (UT 23 November 1993). At the time, this instrument also utilized a 62×58 SBRC InSb array and could be used with a variety of gratings and lenses giving a range of resolutions from $\sim$300 to $\sim$8000. CGS4 is described in Mountain et al. (1990). The 2 μm spectra were obtained using a 75 line/mm grating used in 1st order with the long focal length camera (LFLC) and a 1.5″ wide, 90″ long slit. This resulted in spectral coverage of 2.06 μm to 2.45 μm in two grating positions at a resolving power R=670. The spectra were acquired with an over-sampling of 3× over 2 pixels to fill in gaps in the spectrum caused by the removal of occasional bad pixels. The spectrometer slit was oriented so that spectra of PP 13N and PP 13S were acquired simultaneously. Details of the spectroscopic reduction techniques employed can be found in Puxley, Beard and Ramsey (1992). The bright star BS1203 (B1Ib, K=2.65) was observed in the same configuration as PP 13 and used as a 'ratio star' to cancel atmospheric features. The Brγ absorption feature in BS1203 was removed via linear interpolation prior to ratioing. The absolute flux calibration of the spectra presented below should be considered accurate to $\sim$30%. The spectra of PP 13S, PP 13Na and PP 13Nb are shown in Fig. 2.

2.3. (Sub)mm continuum photometry and mapping

Continuum observations were obtained with the common user bolometer UKT14 on the 15 m JCMT[2], on Mauna Kea, Hawaii, on three different observing runs between August 1990 and October 1992. During the first run (UT 16–18 August 1990) the observing conditions were good and we obtained photometry from 1.3mm to 350 μm. During the second UT 11-12 August 1991) we had similar weather conditions, and we repeated photometry from 1.1mm to 450 μm and obtained one diffraction limited 800 μm map together with several maps at 450 μm. The sky conditions during the third run (UT 16 October 1992) did not permit observations shortward of 1.1mm. All photometry and mapping was carried out with the common user bolometer, UKT14, which is an ^{3}He–cooled, one channel bolometer with a filter wheel and a variable iris that permits diffraction limited observations at wavelength from 1.1mm to 350 μm. For longer wavelengths the optics over–illuminate the primary. The instrument is described in more detail by Duncan et al. (1990). Details of photometry observing techniques and reduction are presented by Sandell (1994).

Continuum maps in on-the-fly mode, i.e. continuously scanning in azimuth while chopping in the scan direction, were obtained at 800 and 450 μm in 1990 and 1991. The chop throw for the 450 μm-maps was 20″ and data were sampled every 2″. The 800 μm-maps were obtained with a chop throw of 40″ and sampled every 4″. The maps were reduced in standard fashion using the NOD2 software package (Haslam 1974). The resultant 450 μm and 800 μm maps of the region are shown in Fig. 3

[2] The James Clerk Maxwell Telescope is operated on a joint basis between the United Kingdom Particle Physics and Astronomy Research Council (PPARC), the Netherlands Organisation for the Advancement of Pure Research (ZWO), the Canadian National Research Council (NRC), and the University of Hawaii (UH).

2.4. ^{12}CO molecular line mapping

The ^{12}CO J=2–1 map was obtained in good weather conditions using the 15 m JCMT telescope on Mauna Kea, Hawaii (UT 13 October 1995) . The total extent of the map was $100''\times 150''$. The mapping was done in on-the-fly mode using the DAS (Digital Autocorrelator Spectrometer) as a backend and RxA2, our 230 GHz SIS receiver, as a frontend. On-the-fly means that the telescope is continuously scanning in the map direction (in this case declination), while the DAS is integrating. To avoid beam-smearing in the scan direction, we used a cell size of $5''$ and a $10''$ step between rows, *i.e.* resulting in a slightly oversampled map. We used a 125 MHz bandwidth, which gives a velocity resolution of 0.1 km s^{-1} and an effective velocity coverage of $\sim$195 km s^{-1}. Most of the map was observed twice and the data were coadded to produce the final map shown in Fig. 4 and binned to 0.2 km s^{-1} resolution.

At 230 GHz, the telescope half power beamwidth, HPBW, is $\sim 21''$, with a measured main beam efficiency $\eta_{\rm mb} = 0.7$. The data are calibrated in antenna temperature using 3-position chopping (hot, cold, sky), and converted the main beam brightness temperatures by dividing the data with $\eta_{\rm mb}$.

3. The Distance to L1473

L1473 is located in the Perseus dark cloud complex, for which the distance estimate is rather uncertain and cover a range from $\sim$ 150–500pc, see e.g. distance reviews by Cernicharo et al. (1985), Ungerechts and Thaddeus (1987), and Cernis (1990). Cohen et al. (1983) quote a distance larger than 140pc for L1473 from photometry of nearby bright stars, but adopt the kinematic distance of 350pc. This distance estimate appears plausible, since L1473 appears to be part of the large California nebula (NGC 1499), which has a distance about 350 pc (Morgan et al. 1953; Ungerechts and Thaddeus 1987).

4. Results

4.1. IR photometry and near-IR spectroscopy

In Fig. 1 we show the NIR J and K band images of the PP 13 region. The images cover an area of sky $\sim 90''$ square and include the sources PP 13S (located at the $0''$,$0''$ of the axes scale), PP 13N (at spatial offset $+8''$,$+14''$) and a field star, (at spatial offset -28$''$,0$''$) henceforth referred to as PP 13W. At J, PP 13S appears diffuse extending some $10''$ in both R.A. and Dec. with a faint, diffuse 'blob' of emission appearing to the north-east of the nebulosity. At K a point-like source is detected at the location of the faint diffuse 'blob' seen at J in the PP 13S nebula . We designate this source PP 13S$*$. The PP 13S nebula is seen to possess two distinct components, *i)* faint diffuse emission extending $\sim 15''$ in both R.A. and Dec., and *ii)* a curving arc of nebulosity surrounding PP 13S$*$.

PP 13N is seen to consist of two components PP 13Na,b at all NIR wavelengths. PP 13Na (the northernmost of the two sources) is considerably brighter than PP 13S$*$ at J with both appearing to be associated with diffuse faint nebulosity. Photometry for all objects in the observed field is given in Table 1. A near-IR colour-colour (J-K vs. H-K) diagram for the sources in the field shown in Fig. 1 is presented in Fig. 2.

Table 1. Near- to mid-IR photometry of PP 13N/S

Filter	S$*$ (3)	S-neb (2)	Na (1)	Nb (4)	W (5)
J	15.68	13.87	12.37	15.09	11.65
H	12.20	12.28	11.24	13.56	10.20
K	9.24	11.10	10.63	12.42	9.61
nbL	6.37	–	9.88	10.74	9.27
M	4.65	–	–	–	–
N	2.58	–	–	–	–
Q	0.06	–	–	–	–
J-H	3.48	1.59	1.13	1.53	1.45
H-K	2.96	1.18	0.61	1.14	0.59
K-L	2.87	–	0.75	1.68	0.34

S$*$ is PP13S$*$; S-neb is PP13S-nebula
Na is PP13Na; Nb is PP13Nb
PP13W is the star west of PP13S$*$ (-30$''$,0$''$) in Fig. 1
Values in () are source IDs in Fig. 2.

Both PP 13S$*$ and PP 13Nb therefore appear to be nebulous and heavily obscured objects. Comparison with earlier photometry shows that PP 13S$*$ is highly variable in the near-IR, varying by about 2 magnitudes at K (Weintraub & Kastner 1992, Tapia et al. 1997). Our photometry of PP 13W would suggest it to be a normal slightly reddened background star, but since Tapia et al. (1997) find it to exhibit Hα and [SII] emission, it is possible that this star is another low-mass PMS star.

Fig. 3 shows the NIR 2 μm spectra of PP 13Na (3a), PP 13Nb (3b) and PP 13S$*$ (3c). All prominent spectral features present in the spectra are identified. PP 13S$*$ (3c) possesses a strong, rising red continuum over this wavelength range which is not surprising since it was barely detected at 1.2 μm. Superposed on the continuum are two main features *i)* molecular hydrogen (H_2) emission in the form of the ro-vibrational v=1–0 S(1) 2.122 μm line, and *ii)* broad ^{12}CO absorption bands starting at 2.294 μm and extended to the edge of the observed wavelength range. One can also see faint NaI and CaI (2.207 μm and 2.264 μm respectively) lines in absorption. No Br-γ emission or absorption was detected on any of the sources in the region. PP 13Na (3a) shows a slowly declining continuum, and possesses *i)* NaI and CaI absorption lines , and *ii)* ^{12}CO absorption bands similar to those in PP 13S$*$, but considerably less broad. Although PP 13Nb (Fig. 3b) is somewhat fainter than the other two sources, we find that it shows a red continuum rising to longer wavelength together with H_2 emission (in the form of the 2.122 μm v=1-0 S(1) line and Q-branch). Even here we detect ^{12}CO bandhead absorption, however, in PP 13Nb the absorption is very weak compared to the same bands in PP 13Na and mostly filled in by H_2 emission longward of 2.4 μm.

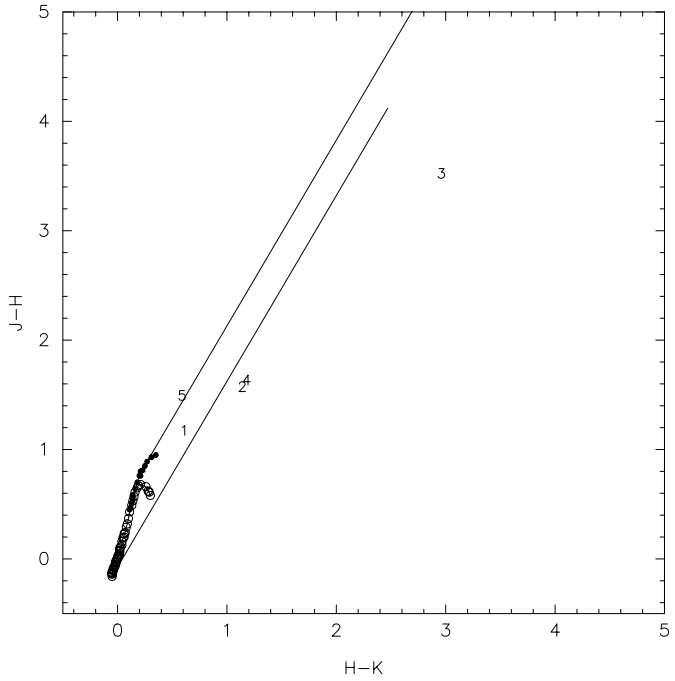

Fig. 2. J-H vs. H-K two colour diagram for the sources in the observed PP 13 field. The location of the sources in the plot are marked by an integer number 1–5 where 1 is PP 13Na, 2 is PP 13Nb, 3 is PP 13S∗, 4 is PP 13S-neb and 5 is the field star PP 13W.

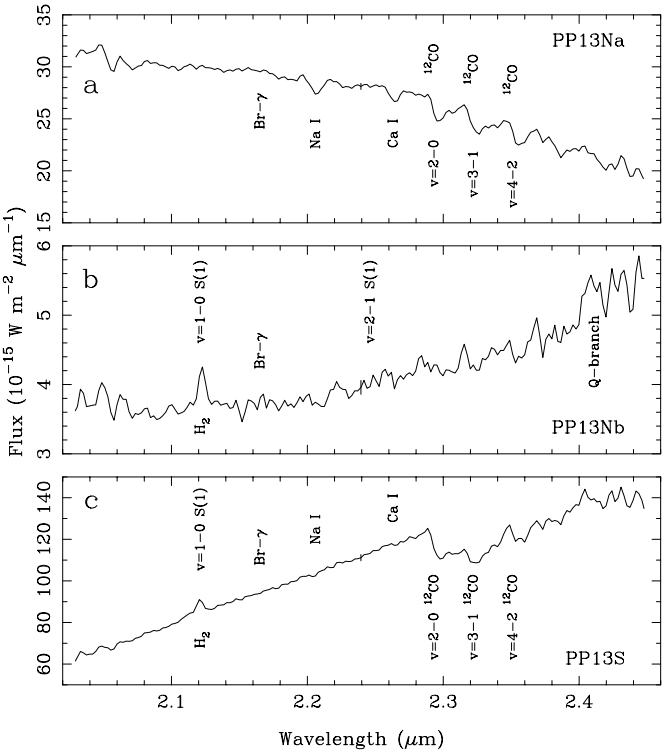

Fig. 3. 2 μm spectra of PP 13Na,b and PP 13S. A representative error bar is shown at the central wavelength point (2.24 μm) of each spectra. The major spectral features seen in each source are identified.

Since we have long-slit 2 μm spectroscopy of the PP 13 sources, we can readily investigate the spatial extent of spectral features along the slit. The slit was oriented such that all three sources, PP 13S∗, PP 13Na and PP 13Nb, were observed simultaneously. Thus, we also obtained spectroscopy of the curving nebulosity south-west of PP 13S∗, of the diffuse region between PP 13S∗ and PP 13Nb, and of the region north-east of PP 13Na. The most interesting feature present in the spectra at the location of both PP 13S∗ and PP 13Nb is the H_2 emission. We find that the H_2 emission is, in fact, strongest in the CGS4 pixel immediately south-west of PP 13S∗. This pixel falls directly on the curving nebulosity seen in Fig. 1 (K band). The H_2 emission weakens on PP 13S∗ itself and disappears completely in the pixel immediately north-east of the source. H_2 emission appears directly on PP 13Nb, weakens in the pixel to the north-east and is no longer present in the spectrum of PP 13Na. Tapia et al. (1997) report that H_2 emission is largely absent in PP 13S from comparing K and narrowband H_2 images obtained in February 1994. If this is the case, the H_2 emission must have faded considerably over a timescale of ~ 3 months. It is more likely, however, that they did not have enough sensitivity to see the relatively faint line emission towards the much brighter continuum background. The λ2.122 μm v=1-0 S(1) line fluxes from PP 13S∗, the curved nebulosity to the south-west and PP 13Nb are given in Table 2.

Table 2. v=1-0 S(1) line fluxes

Source	S(1) Line Flux W m^{-2}
PP13S∗	5.0 10^{-17}
PP13Nb	3.6 10^{-17}
PP13Neb	6.7 10^{-17}

PP13Neb is the curving nebulosity south-west of PP13S∗.

4.2. Radio continuum and line observations

The (sub)mm continuum dust emission peaks within a few arcseconds of PP 13S∗; some fainter emission extends to the north and north-east (Fig. 4). Both continuum maps reveal some continuum emission coincident with PP 13N (consistent with the detection quoted by Osterloh & Beckwith 1995) but our maps are not deep enough and of sufficient spatial resolution to say conclusively whether the emission originates from PP 13Na, PP 13Nb or both sources. The sub-mm emission from PP 13S∗ is clearly extended in both our sub-mm maps. Additional support for this is obtained by comparing a) our multiple photometry values at 800 μm using different apertures (Table 3), b) our broad beam 450 μm (18″) photometry with the calibrated diffraction-limited value (7.8″ beam, see below), and c) our 1.3mm photometry (0.445 Jy/beam; 19.5″ beam) to that of Os-

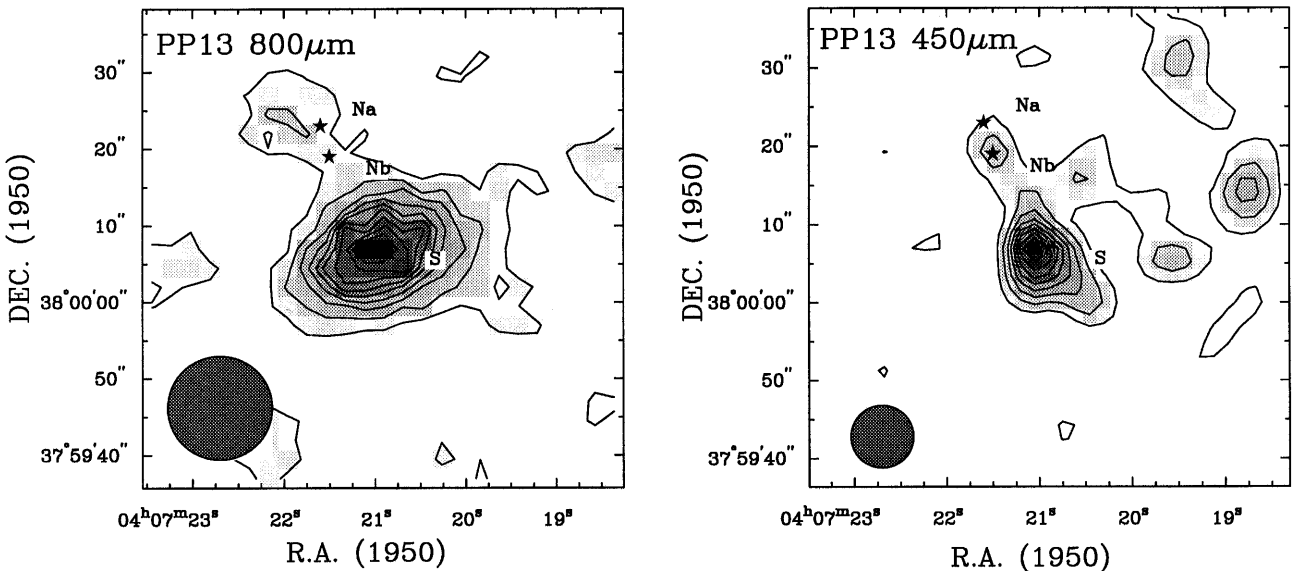

Fig. 4. 800 μm and 450 μm continuum maps of the PP 13 region. PP 13S, Na and Nb are marked. Both the 800 μm and 450 μm emission are extended to both north-east and south-west.

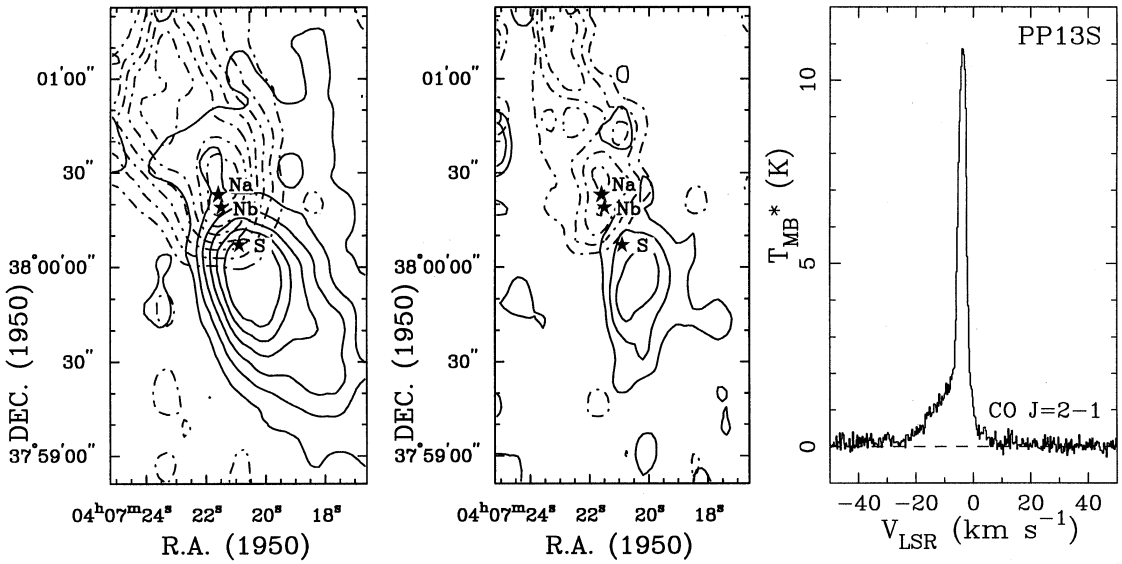

Fig. 5. The first two panels show low- (left) and high- (middle) velocity ^{12}CO J=2–1 emission from PP 13S, while the right-hand panel shows the ^{12}CO spectrum centered on PP 13S. The blue-shifted emission is plotted with solid contours and the red-shifted one with dash-dotted curves. The low-velocity emission map shows the integrated emission over the velocity range -15– -5 & -2–+4 km s^{-1}. The high-velocity map shows the integrated emission over the velocity range -20– -15 & 4–9 km s^{-1}. The location of the source PP 13S$*$ is indicated by the $*$S. PP 13Na and PP 13Nb are marked by $*$Na and $*$Nb. A molecular bipolar outflow is clearly present with the blue-shifted and red-shifted lobes extending to the south-west and north-east, respectively. PP 13$*$ lies close to the intersection of the blue- and red-shifted outflow lobes suggesting strongly that this source is the origin of the outflow.

terloh & Beckwith (0.325 Jy/beam ; 12″ beam). The 800 μm map shows an elliptical source with a FWHM of 14.8″$\times$ 10.0″ with a p.a. of -70° after reducing the data with DBMEM (Richer 1992), but the true size is likely to be smaller. The 450 μm map gives a FWHM of $\sim$ 10″, and the total integrated flux within the central 40″ is $\sim$ 12.5 Jy, while the peak flux in the 7.8″ beam is $\sim$ 5.5 Jy/beam. Assuming that the compact source has a Gaussian distribution with a FWHM of 10″ gives a total flux of 9.8 Jy, suggesting that there is fainter extended dust-emission outside the core region. This is also seen when comparing IRAS point source fluxes with narrow beam KAO data (Cohen et al. 1982), which show that the IRAS fluxes are about 40% higher than the KAO fluxes. The continuum source appears disk-like in the 800 μm map while at 450 μm it appears somewhat more extended along the symmetry axis of the bipolar nebula rather than orthogonal to it, i.e. quite opposite to what is seen at 800 μm. In this case the 450 μm morphology is likely to be an artifact of the restore algorithm, because the 450 μm map is dominated by

Table 3. Sub-mm photometry of PP 13S and N.

Filter/HPBW	Aug 90	Aug 91	Oct 92
PP13S			
1.3mm/19.5"	0.45 ±0.03	–	0.44 ±0.04
1.1mm/18.5"	0.64 ±0.08	–	0.59 ±0.04
800 μm/16.5"	1.56 ±0.13	1.47 ±0.05	–
800 μm/16.5"	–	1.42 ±0.07	–
800 μm/13.5"	–	1.11 ±0.07	–
800 μm/13.5"	–	1.14 ±0.08	–
750 μm/17.5"	–	1.88 ±0.13	–
450 μm/18"	7.89 ±0.94	7.25 ±0.89	–
350 μm/19"	16.2 ±1.7	–	–
PP13N			
1.1mm/18.5" [a]	–	–	0.130 ±0.022

All fluxes are given in Jy/beam.
[a] includes some emission from PP13S.

single raster map. We have found that single continuum maps obtained with small chop throws often results in a symmetric source being more extended orthogonal to the scan direction, rather than parallel to the scan, which is the case for the current 450 μm map.

Fig. 5 show the low-velocity (-10 to -6 km s^{-1} and -1 to +4 km s^{-1}) and high-velocity (-20 to -15 km s^{-1} and +4 to +9 km s^{-1} ^{12}CO emission from the PP 13 region, respectively. Directly on PP 13S (see the ^{12}CO spectrum in Fig. 5), the ^{12}CO emission is strongest on the blue-shifted wing of the line. This is likely due to the fact that the blue-shifted emission lobe of the outflow is seen to extend further over PP 13S than does the red-shifted lobe (see Fig. 5 center panel). It is clear that a bipolar-type molecular outflow emanates from the region containing the near-IR sources. The blue-shifted ^{12}CO lobe extends to the south-west while the red-shifted emission extends to the north-east, as one would expect, given that the nebulosity of PP 13S extends southwards from the star. In total, the ^{12}CO emission is $\sim \pm 2'$ in overall length and, particularly at high-velocities the emission is well collimated.

The CO emission from L1473 has a systemic velocity of about -3.5 km s^{-1} and peaks close to PP 13S. The molecular outflow is clearly centered close to PP 13S, but especially at low velocities (Fig. 5) the outflow lobes overlap. Since PP 13Na,b lie on the symmetry axis of the outflow, it is not directly clear whether PP 13S$*$ or N drives the outflow. At higher velocities, the symmetry of the outflow clearly favour PP 13S$*$. It is possible that PP 13Nb may contribute to the outflow, especially since we see vibrationally excited H_2 emission toward the star. Because the outflow is rather well collimated, the overlap between the blue and the red outflow suggests that the flow is seen with a relatively high inclination. Following Liseau & Sandell (1986), i.e. assuming a conical outflow with constant outflow velocity, we use the aspect ratio and velocity information of the flow to estimate the inclination of the outflow to be *i*=53° with respect to the line-of-sight. Since we have only observed ^{12}CO J=2–1, we have no means of determining the kinetic temperature (T_k) of the outflowing gas, however, if we assume that the gas is optically thin with T_k=20K, we obtain a total mass of $\sim$0.01 $M_\odot$ for both the blue- and for the red-shifted outflow lobes. The momentum of the outflowing gas is 0.14 and 0.10 $M_\odot$ km s^{-1} for the blue and the red flow, respectively (again assuming optically thin emission and with no inclination correction). The momentum flux, F, is $\sim$ 0.015 10^{-5} $M_\odot$ km s^{-1}yr^{-1} for both outflow lobes, while the dynamical time scales are 6.6 10^3 and 5.6 10^3 years again for the blue- and the red-shifted outflow lobes, respectively.

4.3. Modelling the (sub)mm dust emission

The sub-mm emission shows that the dust around PP 13S is extended with a FWHM of $\sim 10''$, corresponding to a physical radius of 2.6 10^{16}cm (1750 A.U.). The first model we use is a simple isothermal model, i.e. we perform a least-squares fit of the observed (sub)mm and far-infrared fluxes, omitting data points shortward of 100 μm where the emission is dominated by hot dust close to the star (but which should have a rather small mass). The only constraint in this fit is that the size of the source is set to 10″. The best-fit model gives a dust temperature T_d=25K, a dust emissivity index, β=1.21 and a total mass of the dust envelope of 0.61 $M_\odot$ assuming the standard Hildebrand-mass opacity of 0.1 cm^2 g^{-1} at 250 μm and a dust to gas ratio of 100 (Hildebrand 1983). This would correspond to a line-of-sight visual extinction of A_V $\sim$100 magnitudes. This is yet another confirmation that the dust most likely resides in a disk rather than spherical envelope.

In fact, as we argue in the discussion, the emission from PP 13S$*$ almost certainly originates from an inclined disk. We have therefore also modelled the spectral energy distribution with a simple disk model (Natta et al. 1993) of the type first introduced by Adams et al. (1988), which has been extensively used for modelling FIR and sub-mm emission of PMS stars. We follow the same convention and characterize the disk temperature and density structure with power law indices *q* and *p*. The former is determined from the spectral energy distribution (SED) between 2 and 60 μm shown in Fig. 6 and gives a value of $q \leq 0.5$, i.e. similar to what is found for most FU Orionis stars (Weintraub et al. 1991), suggesting the presence of an active disk (a value of *q* $\sim$0.75 would suggest a viscous or simple reprocessing disk). We adopt a mass opacity $\kappa_\nu[1.3mm]$=0.02 cm^{2}g^{-1}, approximately the same as used by many others. We perform a least-squares fit of the model to the observed SED but we fix the temperature index *q*=0.5 and the inclination as 45° (cf. Sect. 5.2). Instead of allowing the β-index to vary, we solve the model for several values of β in the range of 1.0–2.0, all of which result in very good fits. This is not surprising, since we have a large number of free parameters, specifically, the bolometric luminosity (L_{bol}), the inner (R_i) and outer (R_o) disk radii, the disk inner surface density (Σ_i, and the power law index for the density gradient, *p* which we allowed to vary between 1.0 and 1.5). For β=1.5

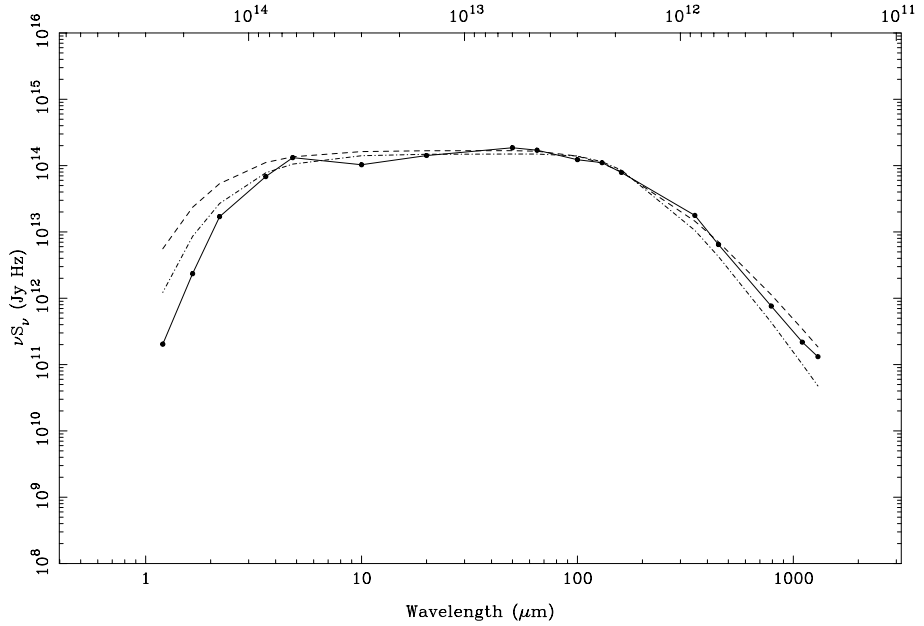

Fig. 6. Spectral energy distribution of PP 13S (solid curve) with model fits from the disk model discussed in the text. The dashed curve is a model fit for β=1.2 while the dash-dot curve corresponds to β=2.0. The poor agreement at short wavelengths is due to the high obscuration in the near-IR, which is not accounted for in our model data.

we derive a disk mass of 0.6 $M_\odot$ with p=1.0, R_i=0.09 A.U. and R_o=2000 A.U.. For β=1.0 we obtain an equally good fit with p=1.0, R_i=0.17 A.U. and R_o=2000 A.U., predicting a disk mass of 1.4 $M_\odot$. The luminosity of the disk in both cases is almost identical (L_{disk}=26 $L_\odot$) and a total luminosity, L_{bol}=30 $L_\odot$. The disk masses we derive are therefore not that different from what we obtained with our simple isothermal model.

We can also compare our results to the results deduced by Osterloh & Beckwith (1995), who use an almost identical mass opacity and temperature index but adopt β=1 and p=1.5. They derive a much lower disk mass of 0.3 $M_\odot$ likely due to the lower value for β, the higher p value and the fact that their derived value for R_o is only 200 A.U. e.g. 10x smaller than our value. Since we know that the sub-mm emission is extended, we corrected our fluxes for a source size of 10″ derived from our 800 μm–map. Such a source size would bring the Osterloh & Beckwith (1995) photometry in agreement with our 1.3mm photometry.

5. Discussion

Both PP 13S$*$ and the double star system PP 13Na,b are heavily reddened stars with nebulosity. PP 13Na, the least obscured of the three stars, was identified as an M2.5 T Tauri star by Cohen et al. (1983). We will demonstrate that all three stars are young low luminosity pre-main sequence stars embedded in the L1473 dark cloud. At least two of the stars, PP 13Nb, and PP 13S$*$ show evidence for outflow activity.

5.1. What is PP 13S$*$?

PP 13S$*$ is a low-luminosity object (L_{bol}=30 $L_\odot$) associated with a compact optical and near-IR nebulosity, that appears to be embedded in the L1473 dark cloud (Cohen et al. 1983). It is an IRAS source associated with variable H_2O maser emission (Persi et al. 1994) and a relatively strong (sub)mm source (Osterloh & Beckwith 1995; this paper). An optical spectrum by Cohen et al. (1983) shows TiO absorption lines and strong [OI] and [SII] emission lines, but no Hα emission. It has an unusually deep 3 and 10 μm absorption bands and is highly variable in the near-IR (Smith 1993; Tapia et al. 1997). Data presented in this paper also shows that it is associated with a CO outflow, that it has vibrationally excited H_2 emission and deep and broad CO overtone band absorption. PP 13S$*$ is therefore either an early M giant (mainly on the evidence that it lacks Hα) or a young low-mass pre-main sequence star (Cohen et al. 1983; Smith 1993; Weintraub & Kastner 1992; Tapia et al. 1997).

There are no grounds for classifying PP 13S as an evolved star. Observational data support the hypothesis that PP 13S is a very young low-mass star. i) The spectral energy distribution of the star is flat between a few microns all the way to 100 μm. This makes the source a classic Class I object in the Adams, Lada and Shu (1987) scheme of young stellar objects. ii) The star is located in a dark cloud with at least one nearby T Tauri star, i.e. there are sign-posts of on-going star formation in the cloud. iii) The luminosity of the star is consistent with a low-mass Class I object and as such is either a very young T Tauri star or an FU Orionis star; the only late-type stars which appear morphologically similar are proto-planetary object. These are already in their AGB evolutionary phase with typical luminosities of 10^4–10^5 $L_\odot$. iv) Sub-mm photometry and mapping confirm that the PP 13S$*$ is associated with an extended, rather massive dust disk/envelope, similar to what is often seen in FU Orionis stars or proto-stellar (Class I objects) driving outflows. In late-type stars the dust emission always appears much more centrally condensed. v) Short term changes in the electron density in the nebulosity (Cohen et al. 1983) signify variations in the stellar wind and are typical in PMS stars, but not in proto-planetaries. vi) Although CO band absorption is present in the spectra of supergiant stars, highly broadened CO absorption (as seen in PP 13S$*$) is one of the clearest signatures of the presence

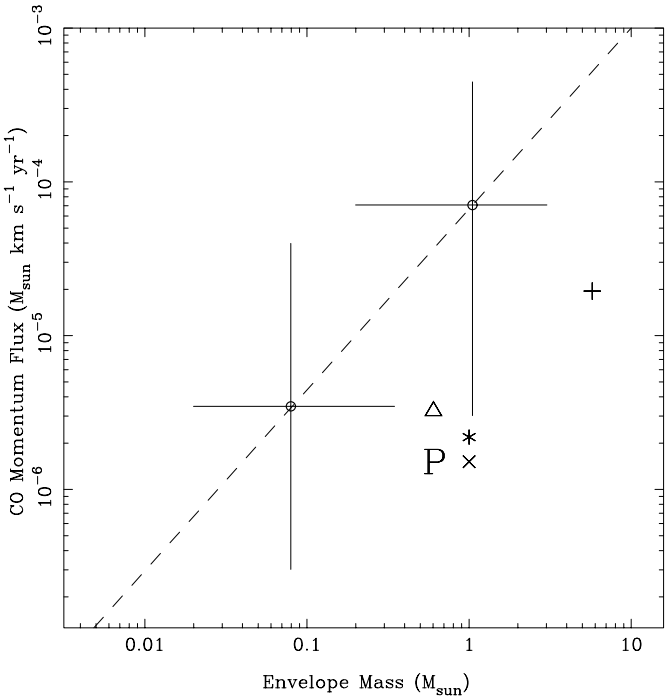

Fig. 7. Plot of the CO momentum flux vs. envelope/disk mass for Class 0 and Class I PMS stars from Bontemps et al. (1996), known FUors (calculated from data in Evans et al. (1994) and PP 13S. The upper-right and lower-left range bars represents the area covered by Class 0 and Class I sources, respectively. The dashed line is the relationship between CO momentum flux and envelope/disk mass derived by Bontemps et al. The symbols represent the location of the FUors and PP 13S in this plot. In all cases the symbol shows the location of the average momentum flux over the red- and blue-shifted outflow lobes. The FUors shown are: RNO1b (+), Elias 1-12 (∗), Z CMa (X) and V346 Nor (triangle). The letter P shows the location of PP 13S. Note that PP 13S lies in a region populated by FUors rather than Class 0 or Class I PMS stars

of an accretion disks especially surrounding FU Orionis stars (Kenyon & Hartmann 1987; Reipurth & Aspin 1997).

5.2. PP 13∗, a typical FUor

FU Orionis stars, (FUors) are young stellar objects that have been seen to suddenly increase in brightness by several magnitudes and then slowly decay over a timescale of several decades (Herbig 1990; Hartmann & Kenyon 1996). After the outburst the spectral type appears to change from being a late type T Tauri star to an early type supergiant. The most likely explanation for the outburst is a rapid mass accretion onto the star, triggered by a thermal instability in the inner, ionized regions of a surrounding accretion disk (Hartmann & Kenyon 1985). The first members of the FUor group were all identified on the basis of optical criteria and optical outbursts, i.e. having a predominantly absorption spectrum resembling an F- or G-type supergiant with broad lines, P Cygni type Hα emission and strong Li I λ6707 absorption. Kenyon et al. (1993) later added the presence of strong CO absorption in the near-IR, which has increased the number of suspected FUors to about 10.

Even though we have not seen an optical outburst from PP 13S∗, it appears to have all the characteristics of a FUor. Morphologically the PP 13S region shows a close resemblance to that of most FUors. The star is associated with a fan-shaped reflection nebula, and has a strong infrared excess, which is commonly seen in FUors. Optical spectroscopy (Cohen et al. 1983) shows strong a red continuum with strong metal absorption lines and [OI] and [SII] lines in emission. As noted by Cohen et al. the star is completely obscured and therefore the spectral features largely originate from the nebulosity with some reflected emission from the star itself. Because the spectra obtained by Cohen et al. have low dispersion, it is not possible to see whether the metal lines are double peaked, which is usually the case for FUors. Li I may be present in absorption, but there is no Hα either in emission or absorption. However, because of the high extinction towards the star, it is likely that most of the Hα emission is absorbed by the dust disk.[3]

At the time Cohen et al. (1983) took their spectra, the [SII] emission was variable with a time-scale of 15 days, suggesting that the [SII] emission originates in the cooling region of a moderately high-velocity shock from a variable stellar wind. The shock velocity has to be high enough to ionize sulphur, but not so high that it would ionize large amounts of hydrogen, i.e. probably about 50 km s^{-1}. Additional support for a strong stellar wind is given by the detection of vibrationally excited H_2 in the near-infrared (this paper). The strongest evidence that PP 13S∗ appears to be an FUor, however, comes from the unusually deep and broad 2 μm CO bandhead absorption. This is very difficult to explain with anything other than an accretion disk. In a recent study of the energy sources of Herbig-Haro (HH) outflows, Reipurth & Aspin (1997) found that a large fraction of these sources showed deep, broadened 2 μm CO bandhead absorption. This was interpreted as evidence of a strong link between HH object production and FUor-type outbursts. If we compare the 2 μm spectrum of PP 13S∗ with the spectra of these sources we find that PP 13S∗ exhibits remarkably similar CO characteristics to the classical FUor V1057 Cyg which shows equally broad CO overtone absorption and is known to possess an inclined accretion disk (Kenyon 1995). An obscuring inclined accretion disk can also explain the deep 3 and 10 μm absorption bands seen in the IR (Cohen et al. 1983, Smith 1993) and the fact that our 2 μm imaging shows the star to be completely invisible in J and only barely visible in H. The only reason we see the star at all is due to the inclination of the disk with respect to the plane of the sky, which we estimate to be $\sim$ 40°. We have made this estimate in three different ways. If we

[3] Optical imaging of PP 13 together with optical spectroscopy of the PP 13S nebula obtained by Aspin & Sandell (in prep.) in October 1997 shows that PP 13S∗ has faded considerably. The optical spectrum showed no significant continuum flux and displays only faint emission lines of Hα and [SII]. This suggests that the intrinsic luminosity of PP 13S∗ may be declining or that the line-of-sight extinction towards it has drastically increased since the observations by Cohen et al (1983) obtained in 1980.

assume that the disk is orthogonal to the CO outflow it should have an inclination $\sim 37°$. If we assume the ellipticity of the 800 μm emission is real and due to projection effects, we derive an inclination of 42° from the aspect ratio. Finally, if we assume that the elliptical arc seen in the K band image is due to emission from the front surface of an inclined circularly symmetric disk, we get 39°, i.e. all three estimates suggest a disk inclination of $\sim 40°$.

Most FUors are found to drive outflows. In their survey of molecular outflows from FUors, Evans et al. (1994) found CO outflows in 6 of the 8 stars searched with typical dynamical timescales and outflow masses very similar to what we find for PP 13S$*$. Bontemps et al. (1996), in their study of outflow properties of Class I and 0 objects find a close correlation between momentum flux and envelope mass of young stars. It is therefore interesting to see how PP 13S$*$ and other FUors fit into this scheme. If we use the same correction factors that Bontemps et al. adopted, i.e. a factor of 3.5 for optical depth correction and an inclination of 57.3° i.e. a total correction factor of 10 for momentum flux, we obtain F(PP 13$*$)=0.153 and 0.146 $10^{-5}\,M_\odot$ km $s^{-1}yr^{-1}$ for the red- and blue-shifted CO outflows, respectively. The envelope (disk) mass and bolometric luminosity clearly places PP 13$*$ in the upper end of Class I sources, in the area mostly populated by Class 0 sources, while the momentum flux falls below their 'best-fit' correlation by at least a factor of 5. Although Evans et al. do not directly compute momentum flux for their sample, they give enough details that we can derive it in the same we as we did for PP 13S$*$. We use their mass and momentum estimates derived for optically thin CO but note that the optical depth corrections they derive are close to the value recommended by Cabrit & Bertout (1992) and what was used by Bontemps et al. (1996). We take the envelope or disk masses from Weintraub et al. (1991), but recalculate the masses in the same manner as we did for PP 13$*$. Fig. 7 shows that FUors tend to show a rather tight correlation between momentum flux and disk mass, but the momentum flux is almost a factor of 10 lower than what one would expect from the correlation by Bontemps et al. This implies that the FUor accretion disks are much less efficient in driving outflows than the disks surrounding Class 0 or Class I sources. The momentum flux from the PP 13S outflow is found to lie in the same regime of the figure as the FUors supporting its interpretation as a member of this class of objects.

References

Adams, F.C., Lada, C.J., & Shu, F.H., 1987 ApJ, 321, 788
Adams, F.C., Lada, C.J., & Shu, F.H., 1988 ApJ, 326, 865
Beckwith, S.V.W., & Sargent, A. I., 1991 ApJ, 381, 250
Bontemps, S., André, P., Terebey, S., & Cabrit, S., 1996, A&A, 311, 858
Cabrit, S., & Bertout, C., 1992, A&A, 261, 274
Cernis, K., 1990 Ap & Sp Sc, 166, 315
Cernicharo, J., Bachiller, R., & Duvert, G., 1985 A&A, 149, 273
Cohen, M., Aitken, D.K., Roche, P.F., & Williams, P.M., 1983 ApJ, 273, 624
Duncan, W.D., Robson, E.I., Ade, P.A.R., Griffin, M.J., Sandell, G., 1990, MNRAS, 243, 126
Evans II, N.J., Balkum, S., Levrault, R.M., Hartmann, L., & Kenyon, S., 1994, ApJ, 424, 793
Hartmann, L., & Kenyon, S.J., 1985, ApJ, 299, 462
Hartmann, L., Kenyon, S.J., & Hartigan, P., 1993 in Protostars and Planets III, Eds E.H. Levy & J. Lupine (Tucson: Univ. Arizona), 497
Hartmann, L., & Kenyon, S.J., 1996, ARA&A, 34, 207
Haslam, C.G.T., 1974, A&AS, 15, 333
Herbig, G.H., 1989 in ESO Workshop on Low Mass Star Formation and Pre-main-sequence Objects, Ed. Bo Reipurth (Garching, ESO), 233
Hildebrand, R.H., 1983, Quart.J.R.A.S., 24, 267
Kenyon, S.J., & Hartmann, L., 1987, ApJ, 312, 243
Kenyon, S.J., Hartmann, L., Gomez, M., Carr, J.S., & Tokunaga, A., 1993, AJ, 105, 1505
Kenyon, S.J., 1995, A&SS, 223, 3
Liseau, R., & Sandell, G., 1986, ApJ, 304, 459
Morgan, W.W., Whitford, A.E., & Code, A.D., 1953 ApJ, 118, 318
Mundt, R., Brugel, E.W., & Bührke, T., 1987, ApJ, 319, 275
Natta, A., Palla, F., Butner, H.M., Evans, II N.J., Harvey, P.M., 1993, ApJ, 406, 674
Osterloh, M., & Beckwith, S. V. W., 1995, ApJ, 439, 288
Parsamian, E.S., & Petrossian, V. M., 1979, *Akad. Nauk. Armenian SSR, Soobscheniia*, No.**135**, Erevan
Reipurth, B., Aspin, C., 1997, AJ, 114, 2700
Richer, J.S., 1992, MNRAS, 254, 165
Sandell, G., 1994, MNRAS, 271, 75
Saraceno, P., André, P., Ceccarelli, C., Griffin, M., Molinari, S., 1996, A&A, 309, 827
Smith, R.G., 1993, MNRAS, 264, 587
Tapia, M., Persi, P., Bohigas, J., & Ferrari-Toliolo, M., 1997, AJ, 113, 1769
Ungerechts, H., Thaddeus, P., 1987, ApJ Suppl., 63, 645
Weintraub, D.A., Sandell, G., & Duncan, W.D., 1989, ApJ, 340, L69
Weintraub, D.A., Sandell, G., & Duncan, W.D., 1991, ApJ, 382, 270
Weintraub, D.A., & Kastner, J.H., 1992, BAAS, 24, No. 4, 1141